Coarse-Grid Simulation of Gas-Particle Flows in Vertical Risers

Arthur T. Andrews IV, Peter N. Loezos, and Sankaran Sundaresan*

Department of Chemical Engineering, Princeton University, Princeton, New Jersey 08544-5263

Continuum model equations for unsteady gas-particle flows in devices such as fluidized beds and circulating fluidized bed risers contain unstable modes whose length scale is of the order of 10 particle diameters. Yet, because of limited computational resources, these flows are routinely simulated by solving the discretized version of continuum models over coarse spatial grids. These simulations resolve the large-scale flow structures but not the finer scale structures. In most industrial applications involving large devices, it is impractical to resolve all the fine-scale structures, and therefore the effects of the unresolved structures must be addressed through suitable subgrid models. Using gas-particle flows in a wide and very tall vertical channel as an example, we have demonstrated in this study that the results obtained in coarse-grid integration of the microscopic equations for gas-particle flows change appreciably if subgrid corrections to account for the effects of unresolved structures are included. The addition of a simple time-averaged subgrid closure for the effective drag coefficient and particle phase viscosity and pressure led to a qualitative change in the simulation results. Our simulations also revealed a lack of separation of time scales between the resolved and unresolved structures. This led us to formulate a simple stochastic subgrid closure for the drag coefficient and investigate its consequence. The addition of a stochastic correction made quantitative, but not qualitative, changes to the simulation results.

Introduction

Gas-particle flows in vertical risers are inherently unstable, and they manifest fluctuations over a wide range of length and time scales. There is a substantial body of literature where researchers have sought to capture these fluctuations through numerical simulation of continuum equations for gas-particle flows.[1−17] Continuum models for such flows, coupled with either simple phenomenological closures for drag and effective stresses[18] or closures obtained by extending the kinetic theory of granular materials to account for the presence of the interstitial fluid,[9,19,22] reveal unstable modes whose length scale is as small as 10 particle diameters (see Appendix A for further discussion of the unstable modes). Yet, because of limited computational resources, riser flows in large units are often simulated by solving discretized versions of the continuum model equations over a coarse spatial grid. Such coarse grid simulations do not resolve the small-scale (i.e. subgrid scale) spatial structures which, according to the continuum equations, do indeed exist. The extent to which these unresolved structures affect the resolved structures is an open question.[21]

Such unresolved structures commonly arise in single phase turbulent flow, where large eddy simulations strive to incorporate the influence of the unresolved structures on those resolved in the simulations through subgrid models; however, such subgrid corrections have not received much attention in the context of heavily loaded gas-particle flows. In the present study, we have examined the influence of the unresolved structures on the resolved flow characteristics of gas-particle flows at appreciable mass loading of particles, using two-dimensional simulations of flows in a vertical channel as the model problem. We have accounted for the consequences of the unresolved structures on the drag coefficient and the particle phase stresses through computationally generated closures which are limited to the specific test problem considered. By comparing results obtained from coarse-grid simulations with and without the subgrid closures, we expose the large effects that the unresolved flow structures can have on the resolved flow characteristics.

Agrawal et al.[20] have examined in detail the fate of a uniform suspension of particles fluidized by a gas through highly resolved simulations of continuum model equations in two-dimensional (2-D) and three-dimensional (3-D) periodic domains, whose size is of the order of the typical grid sizes employed in coarse-grid simulation of large scale risers and fluidized beds. In their analysis, they employed a kinetic theory closure for the particle phase stress[9,19,22] and a drag force model proposed by Wen and Yu.[23] They found that the uniformly fluidized state was unstable and that it quickly gave way to persistent, time-dependent, mesoscale structures, which assumed the form of clusters and streamers at low particle volume fractions and bubbles at high particle loadings. They found that the effective drag coefficient obtained by averaging the results over the periodic domain (a) was appreciably smaller than that corresponding to a homogeneous state, (b) was dependent on the size of the domain, and (c) manifested a rather complex but understandable dependence on particle volume fraction. They also found that the effective viscosity of and the normal stresses in the particle phase obtained by averaging over the mesoscale structures were (a) appreciably larger than those corresponding to the homogeneously fluidized state (given by the kinetic theory) and (b) depended on the size of the domain. Based on these findings, they concluded

* To whom correspondence should be addressed. E-mail: sundar@princeton.edu.

10.1021/ie0492193 CCC: $30.25
Published on Web 04/05/2005

that unresolved mesoscale structures could contribute appreciably to results predicted by coarse-grid simulations.

The purpose of the present study is to assess the influence of unresolved structures on the results obtained in coarse-grid simulations of gas-particle flows. We will demonstrate in this paper that the expressions for the drag coefficient and the particle phase effective viscosity and pressure used in the coarse-grid simulations should account for the influence of the unresolved (subgrid) structures and that because of a lack of separation of time scales between resolved and unresolved structures one should, in a strict sense, employ stochastic subgrid closures for these quantities. However, simple deterministic subgrid closures seem to capture much of the large-scale flow structures obtained with stochastic subgrid closures.

It has long been recognized in industrial practice that CFD simulations based on averaged equations of motion underestimate the holdup in fluidized beds and riser flows, unless an apparent particle cluster size (typically two to 10 times the true size of the particles) is used in the calculations. Such a larger cluster size leads to a smaller drag coefficient than what would be obtained if the true particle size is employed. Thus, one can indeed view the use of an apparent particle cluster size as a simple subgrid closure for the drag coefficient. Apparent cluster size is sometimes used as a tuning parameter to match the simulation results with experimental data.[24] A method to estimate the cluster size via an energy-minimization-multiscale model has been presented in the literature recently.[25] O'Brien and Syamlal[26] and Boemer et al.[27] pointed out over a decade ago the need for a subgrid closure for the drag coefficient to account for the effect of unresolved clusters. In the present study, we construct deterministic and stochastic subgrid scale closures through fine-grid simulations and examine the impact of these closures on the macroscale flow patterns obtained in coarse grid simulations.

Approach to Coarse-Grid Simulations

The purpose of the simulations described in this study is to examine the flow behavior of a gas-particle suspension in a vertical channel, whose geometrical details are presented later. The starting point of the analysis is a kinetic theory based continuum model for gas-particle flow, see Table 1 (and Appendix B for a brief description). A detailed discussion of these equations can be found in Agrawal et al.[20] and will not be repeated here. This model consists of continuity and momentum equations for the gas and particle phases and an additional scalar equation for the fluctuation energy per unit mass of the particle phase. Henceforth, we will refer to these equations as microscopic (or kinetic theory) equations. Table 2 shows typical particle and gas properties. According to this system of microscopic equations, homogeneously fluidized suspensions (with properties shown in Table 2) are unstable with dominant instabilities occurring at a length scale of the order of 10 particle diameters.[28] We consider only those situations, where the dimensions of the riser are too large to make numerical simulations with grid sizes of the order of 10 particle diameters impractical even in two-dimensional simulations. (Virtually every commercial or medium-scale pilot unit falls in this category.) Consequently, if one carries out coarse-grid integration of these microscopic equations employing a practically affordable grid resolution, there are bound to be small structures which have not been resolved and whose influence is not properly recognized in the simulations. This rather obvious point is well-known in the literature on single-phase turbulent flow and turbulent flow with very dilute loading of particles. Yet, very little has been done about the subgrid scale modeling in the context of gas-particle flows with high mass loading of particles. In this manuscript we compare results obtained in simulation of the microscopic equations discretized using coarse grids with those obtained in coarse grid simulations where the microscopic equations have been augmented with subgrid closures of different levels of sophistication.

A question of fundamental importance in two-phase flows problems is the accuracy of the postulated microscopic equations in capturing the microscale physics behind the flow. The present study does not address this question. Instead, we begin with a reasonable set of microscopic equations developed in the literature, which captures the known instabilities in simple test problems, and examine issues associated with the integration of this *given* set of equations using coarse grids.

Agrawal et al.[20] have already pointed out that the origin of the small-scale structures in gas-particle flows through risers is very different from those in single-phase turbulent flow. In the latter, the small-scale eddies are dissipative and are largely sustained by energy cascade from larger eddies. In contrast, small-scale structures arise in riser flows primarily through local instabilities associated with fluidization; energy to sustain these structures comes largely from the mean relative motion between the particle and gas phases. Consequently, one should not directly apply the subgrid models, which have been developed in single-phase turbulent flows, to the riser flow problem. Agrawal et al.[20] proposed a simple, preliminary approach to generate ad hoc closures for the coarse-grid simulations through highly resolved simulations of the microscopic equations in small periodic domains which are commensurate with the grid sizes to be used in the coarse-grid simulations. This is precisely the approach we have examined here.

Although all the results will be presented in dimensionless form, it is useful to first present some quantities, such as riser dimensions and typical grid size that would be employed in coarse grid simulations, to motivate the specific combination of dimensionless variables employed in our test simulations. The vertical channel through which the gas-particle mixture flows is 76 cm wide and 30 m tall. In the coarse-grid simulation of flow described in this manuscript, the riser is discretized using 2 cm $\times$ 8 cm grids. These are fairly typical of industrial scale risers whose diameters range from 0.5 to 2.0 m and height ranges from 20 to 90 m. Three-dimensional simulations invariably employ even coarser grids.

The microscopic equations were made dimensionless using particle density (ρ_s), terminal velocity (v_t), and (v_t^2/g) as characteristic density, velocity, and length (as in ref 20). It then follows that the characteristic time and stress are (v_t/g) and ($\rho_s v_t^2$), respectively. The particle size then appears in the microscopic equations as dg/v_t^2 ($= 1/\mathrm{Fr_p}$). The aspect ratio of the grid, vertical height (Δ_v)/horizontal width (Δ_h), is denoted by A. The width of the grid in dimensionless form is $\Delta_h g/v_t^2$ ($= 1/\mathrm{Fr_h}$). Using the dimensional quantities presented above as an illustration, $A = 4$, $\mathrm{Fr_p} \sim 65$, and $\mathrm{Fr_h} \sim 0.2434$. The larger

Table 1. Model Equations for Gas–Particle Flows

$$\frac{\partial \rho_s \phi}{\partial t} + \nabla \cdot (\rho_s \phi \mathrm{v}) = 0 \tag{1}$$

$$\frac{\partial (\rho_g (1-\phi))}{\partial t} + \nabla \cdot [\rho_g (1-\phi)\mathrm{u}] = 0 \tag{2}$$

$$\left[\frac{\partial (\rho_s \phi \mathrm{v})}{\partial t} + \nabla \cdot (\rho_s \phi \mathrm{vv})\right] = -\nabla \cdot \sigma_s - \phi \nabla \cdot \sigma_g + \mathrm{f} + \rho_s \phi \mathrm{g} \tag{3}$$

$$\left[\frac{\partial (\rho_g (1-\phi)\mathrm{u})}{\partial t} + \nabla \cdot (\rho_g (1-\phi)\mathrm{uu})\right] = -(1-\phi)\nabla \cdot \sigma_g - \mathrm{f} + \rho_g (1-\phi)\mathrm{g} \tag{4}$$

$$\left[\frac{\partial \left(\frac{3}{2}\rho_s \phi T\right)}{\partial t} + \nabla \cdot \left(\frac{3}{2}\rho_s \phi T v\right)\right] = -\nabla \cdot \mathrm{q} - \sigma_s : \nabla \mathrm{v} + \Gamma_{slip} - J_{coll} - J_{vis} \tag{5}$$

Gas-phase stress tensor

$$\sigma_g = \rho_g \mathrm{I} - \hat{\mu}_g \left[\nabla \mathrm{u} + (\nabla \mathrm{u})^T - \frac{2}{3}(\nabla \cdot \mathrm{u})\mathrm{I}\right] \tag{6}$$

Gas-particle drag (Wen and Yu[23] and Gidaspow[9])

$$\mathrm{f} = \beta(\mathrm{u} - \mathrm{v});\ \beta = \frac{3}{4} C_D \frac{\rho_g (1-\phi)\phi |\mathrm{u} - \mathrm{v}|}{d} (1-\phi)^{-2.65} \tag{7}$$

$$C_D = \begin{bmatrix} \frac{24}{Re_g}(1 + 0.15 Re_g^{0.687}) & Re_g < 1000 \\ 0.44 & Re_g \geq 1000 \end{bmatrix};\ Re_g = \frac{(1-\phi)\rho_g d |\mathrm{u} - \mathrm{v}|}{\mu_g}$$

Particle phase stress

$$\sigma_s = [\rho_s \phi (1 + 4\eta\phi g_o) T - \eta \mu_b (\nabla \cdot \mathrm{v})]\mathrm{I} - \left(\frac{2+\alpha}{3}\right)\left\{\frac{2\mu^*}{g_o \eta (2-\eta)}\left(1 + \frac{8}{5}\phi\eta g_o\right)\left(1 + \frac{8}{5}\eta(3\eta - 2)\phi g_o\right) + \frac{6}{5}\eta\mu_b\right\}\mathrm{S} \tag{8}$$

where $\mathrm{S} = \frac{1}{2}(\nabla \mathrm{v} + (\nabla \mathrm{v})^T) - \frac{1}{3}(\nabla \cdot \mathrm{v})\mathrm{I}$

$$\mu^* = \frac{\mu}{1 + \frac{2\beta\mu}{(\rho_s \phi)^2 g_o T}};\quad \mu = \frac{5\rho_s d\sqrt{\pi T}}{96}$$

$$\mu_b = \frac{256\mu\phi^2 g_o}{5\pi};\ \eta = \frac{(1+e_p)}{2};\ g_o = \frac{1}{1 - (\phi/\phi_{max})^{1/3}};\ \phi_{max} = 0.65;\ \alpha = 1.6$$

Pseudothermal energy flux

$$\mathrm{q} = -\frac{\lambda^*}{g_o}\left\{\left(1 + \frac{12}{5}\eta\phi g_o\right)\left(1 + \frac{12}{5}\eta^2(4\eta - 3)\phi g_o\right) + \frac{64}{25\pi}(41 - 33\eta)\,\eta^2 \phi^2 g_o^{\,2}\right\}\nabla T \tag{9}$$

where $\lambda^* = \dfrac{\lambda}{1 + \frac{6\beta\lambda}{5(\rho_s\phi)^2 g_o T}};\ \lambda = \dfrac{75\rho_s d\sqrt{\pi T}}{48\eta(41 - 33\eta)}$

Rate of dissipation of pseudothermal energy through collisions

$$J_{coll} = \frac{48}{\sqrt{\pi}}\eta(1-\eta)\frac{\rho_s \phi^2}{\mathrm{d}} g_o T^{3/2} \tag{10}$$

Effect of fluid on particle phase fluctuation energy (Koch and Sangani[19])

$$J_{vis} = \frac{54\,\phi\mu_g T}{d^2} R_{diss} \text{ where}$$

$$R_{diss} = 1 + \frac{3\phi^{1/2}}{\sqrt{2}} + \frac{135}{64}\phi \ln\phi + 11.26\phi\,(1 - 5.1\phi + 16.57\phi^2 - 21.77\phi^3) - \phi g_o \ln(0.01) \tag{11}$$

$$\Gamma_{slip} = \frac{81\phi\mu_g^{\,2}|\mathrm{u} - \mathrm{v}|}{g_o d^3 \rho_s \sqrt{\pi T}}\Psi \text{ where} \tag{12}$$

$$\Psi = \frac{R_d^{\,2}}{(1 + 3.5\phi^{1/2} + 5.9\phi)}$$

$$R_d = \begin{bmatrix} (1 + 3(\phi/2)^{1/2} + (135/64)\phi\ln\phi + 17.14\phi/1 + 0.681\phi - 8.48\phi^2 + 8.16\phi^3),\ \phi < 0.4 \\ \frac{10\phi}{(1-\phi)^3} + 0.7,\ \phi \geq 0.4 \end{bmatrix}$$

Table 2. Physical Properties of Gas and Solids

d	particle diameter	7.5×10^{-3} cm
ρ_s	particle density	1.5 g/cm^3
ρ_g	gas density	1.3×10^{-3} g/cm^3
μ_g	gas viscosity	1.8×10^{-4} g/cm·s
e_p	coefficient of restitution	0.9
v_t	terminal settling velocity	21.84 cm/s
v_t^2/g	characteristic length	0.487 cm
v_t/g	characteristic time	0.0223 s
$\rho_s v_t^2$	characteristic stress	715.5 g/cm.s^2

the difference between Fr_p and Fr_h, the more important the contributions of the subgrid corrections will be. Indeed, Agrawal et al.[20] found that as Fr_h decreased, the effects of the mesoscale structures assumed greater and greater importance.

Simulations To Estimate Subgrid Corrections

Agrawal et al.[20] proposed that, as an initial approach to constructing subgrid closures, one perform highly resolved simulations of the microscopic equations in small periodic domains, whose dimensions are commensurate with the grid dimensions of the planned coarse-grid simulations. Such calculations begin with a uniformly fluidized suspension of particles and simulate the evolution of nonuniform structures through instabilities inherent to the fluidization problem. Details of such simulations are described in ref 20, and will not be repeated here. We simply note that all the computations described in the present study were performed using the MFIX code,[29,30] which is based on discretization using staggered grids and a finite volume method. Spatial and temporal derivatives were approximated using a second-order discretization scheme and an implicit Euler scheme, respectively. In all our simulations, we employed the Superbee method to determine the downwind factor, which has been found to yield satisfactory shapes for the nose of bubbles even at only modest grid resolution.[31]

As nonuniform structures evolve, the gas will bypass regions rich in particles, and the domain-averaged slip velocity between the gas and the particles (defined as the difference between domain average values of volume fraction-weighted gas and particle phase velocities) required to support the weight of the particles will take on a larger value than that for the uniformly fluidized state. The nonuniform structures are dynamic in nature, and so will the domain-average slip velocity be. This is illustrated in Figure 1, which presents the instantaneous domain-averaged dimensionless slip velocity as a function of dimensionless time in one such periodic domain calculation. In such simulations, the pressure drop across the bed is chosen to balance the weight of the suspension, and therefore the instantaneous domain-averaged dimensionless drag coefficient (defined such that the domain-averaged dimensionless drag coefficient multiplied by the domain-averaged dimensionless slip velocity is the effective dimensionless drag force per unit volume in the domain) can readily be extracted from the results shown in Figure 1. It can be seen from Figure 1 that after an initial transient period, the flow settles into a statistical steady state with persistent fluctuations. By averaging the results obtained in the statistical steady state, one can obtain a time-averaged value for the domain-averaged slip velocity (shown by the horizontal line in this figure) and then a corresponding time-averaged value for the domain-averaged drag coefficient.

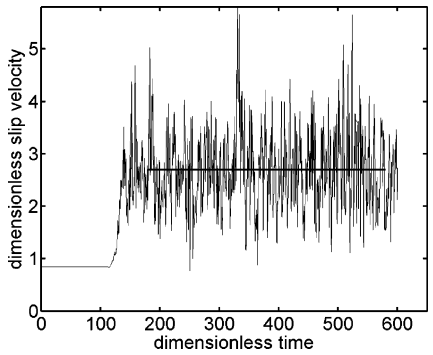

Figure 1. Domain-averaged dimensionless slip velocity calculated in a doubly periodic domain with $Fr_h = 0.2434$; $A = 4$; average particle volume fraction in the domain = 0.05; Reynolds number based on particle diameter and terminal settling velocity, $Re_p = 1.18$. Highly resolved simulation of flow in this periodic domain was performed using 32×128 grids. Time-averaged slip velocity shown as a superimposed line and was calculated between 200 and 800 dimensionless time units. The imposed shear rate in the periodic domain is zero. See ref 20 for details on the introduction of macroscale shear in the periodic domain calculations. The dominant period of the oscillations is ~10 dimensionless units of time. For the parameter values listed in Table 2, this translates to a period of 0.223 s.

Agrawal et al.[20] have already examined the dependence of the time-averaged values of the domain-averaged quantities on the grid resolution used in the simulations; we simply note here that we employed 32×128 grids in the simulations presented in figure, which was found to be adequate by Agrawal et al.[20]

By repeating simulations of the type shown in Figure 1 for different average particle volume fractions in the domain and imposed shear rates, one can create a look-up table or a simple curve-fit function for the time-averaged drag coefficient in terms of the average particle volume fraction and dimensionless shear rate. We found the shear dependence of the effective drag coefficient to be weak for typical shear rates encountered in riser flows, and hence we assumed that the effective drag coefficient was only a function of the particle volume fraction in the domain. This function will change with Fr_h; however, the value of Fr_h was not changed in our simulations. Agrawal et al.[20] found that the domain-averaged quantities had only a weak dependence (if any) on the aspect ratio, A, for $A > \sim 4$. In all our coarse grid simulations, A was four.

Agrawal et al.[20] proposed the use of the look-up table or the curve-fit function for the effective (time-averaged) drag coefficient discussed in the previous paragraph in coarse-grid simulations, as a simple closure for the effect of the unresolved structures on the interphase interaction force. Such a subgrid closure is necessarily ad hoc, as it does not contain any capability to predict how the closure should be modified when the grid size or the particle properties are changed; nevertheless, such an ad hoc closure is adequate to develop a qualitative understanding of the possible influence of unresolved structures on the resolved flow characteristics. We have examined the impact of such a subgrid closure for drag coefficient in our coarse-grid simulations (described later).

This approach has its limitations; for example, in the vicinity of boundaries such as solid walls one would expect that the subgrid closures should be modified to account for the limitations imposed on the fluctuations by the presence of the boundary. Indeed, in LES of single phase turbulent flows, the wall regions are

Table 3. Computationally Generated ad hoc Subgrid Closure for Various Dimensionless Quantities

$$P_{s,meso} = 1.54\phi \exp(-0.701|\tilde{\gamma}|)$$

$$\mu_{s,meso} = \begin{bmatrix} (0.0121|\tilde{\gamma}|^3 - 0.0605|\tilde{\gamma}|^2 + 0.0314|\tilde{\gamma}| + .130)\dfrac{\phi}{0.398} \text{ for } |\tilde{\gamma}| < 2.45 \\ 0.0546\phi \text{ for } |\tilde{\gamma}| \geq 2.45 \end{bmatrix}$$

$$\bar{\beta} = \left(1 - \frac{\rho_g}{\rho_s}\right)\phi(1-\phi)F, \text{ where}$$

$$F = \begin{bmatrix} (396\phi^2 - 30.8\phi + 1) \text{ for } \phi < 0.0375 \\ (.332(1-\phi)^{-5}) \text{ for } \phi \geq 0.0375 \end{bmatrix}$$

treated through wall functions.[32] Our understanding of coarse-grid simulations of gas-particle flows has not evolved to a point where we can begin to address such wall effects; indeed, the extent of influence that subgrid closures can have on the resolved flow fields is not widely studied in this class of problems. In the present study, which is an initial effort to gauge this influence, we have applied the same subgrid closure everywhere in the flow domain and do not treat the wall region separately. We believe that this is a reasonable first approximation, as fluctuations in gas-particle flows in risers (unlike single phase turbulent flows) do not appear to be driven by shear at bounding surfaces—more on this later.

Note that the instantaneous domain-averaged slip velocity, and hence the instantaneous domain-averaged drag coefficient, fluctuate with time, and the basis for using time-averaged values for these quantities to construct a subgrid closure is reasonable if and only if the characteristic fluctuation time scale observed in the coarse-grid simulation is much larger than that in the subgrid calculations illustrated in Figure 1. When a clear separation of time scales does not exist, the consequences of the fluctuating drag coefficient seen in the statistical steady state (illustrated in Figure 1) should be brought into the coarse-grid simulations. We will, however, begin with time-averaged subgrid closures and evaluate if separation of time scale exists or not.

As discussed in detail by Agrawal et al.,[20] one can also extract effective particle phase normal stresses in the vertical and lateral directions and effective particle phase viscosity from such highly resolved simulations. Once again, one can raise the issue as to whether time-averaged subgrid closures for these quantities (which take the form of look-up tables or curve-fit functions) are adequate if there is no clear separation of time scales.

Table 3 contains the time-averaged subgrid closures for the specific values of Fr_h and A used in our illustrative examples. The effective dimensionless drag coefficient, $\bar{\beta}$, is simply a function of local particle volume fraction, i.e., $\bar{\beta} = \bar{\beta}(\phi)$, where ϕ is the instantaneous volume fraction of particles at any node in the coarse grid simulation (and equal to the average volume fraction of particles in the domain in the subgrid closure calculations described in this section). At very low particle volume fractions, an increase in particle volume fraction leads to larger and denser clusters, which decrease the effective drag coefficient, and this regime is captured by an expression where the effective drag coefficient decreases with increasing particle volume fraction. Beyond some threshold level of particle volume fraction, cluster−cluster interactions hinder the relative motion between the clusters and the gas, and, in this regime, the effective drag coefficient increases with increasing particle volume fraction. The time-averaged dimensionless subgrid horizontal normal stress and effective subgrid particle phase viscosity ($P_{s,meso}$ and $\mu_{s,meso}$, respectively) depended both on ϕ and the prevailing macroscale shear rate (see expressions in Table 3, where $|\tilde{\gamma}|$ denotes dimensionless $|dv_y/dx|$, where v_y is the dimensionless vertical velocity and x is the dimensionless lateral position). Both of these quantities decreased with increasing shear rate, indicating a tendency of the shear to orient the clusters and hinder their lateral fluctuations. This shear dependence is exactly opposite of what one obtains in single-phase turbulent flows where subgrid viscosity and stresses increase with shear rate.

We reemphasize that the expressions described here are simple ad hoc subgrid closures. Fundamentally based models for the subgrid corrections are certainly more desirable and should indeed be developed. However, the goal of the present study is to investigate if the inclusion of subgrid closures affects the predicted results in a significant way, thus establishing whether a need exists for an in-depth study of subgrid models in the future. This goal can be achieved using the ad hoc subgrid closures presented in Table 3. We will demonstrate below that subgrid closures do affect the predicted results profoundly.

Coarse-Grid Simulations of Riser Flow

We have performed two-dimensional coarse-grid simulations of gas-particle flows in a vertical channel equipped with a horizontal splash plate at the top, shown schematically in Figure 2. [While 3-D simulations are more desirable, the computational costs are prohibitive. Unlike single phase turbulent flow, nonuniform structures in the gas-particle flow studied here arise primarily through local instabilities, which are already captured in 2-D analysis. Indeed, Agrawal et al.[20] have shown that both 2-D and 3-D simulations of flows in small periodic domains yield similar results, so that there is some reason to expect that the 2-D and 3-D coarse-grid simulations will also lead to similar findings.] Gas and particles entered the channel at the bottom and exited through two symmetric openings on the sides, located near the top of the riser. The exit pressure (in dimensional units) was set to be atmospheric. The gas and particle interstitial velocities at the inlet were *independent* of lateral position and equal to 27.47 and 16.67 dimensionless units, respectively. The particle volume fraction at the inlet was set to be 0.04. The compressibility of gas was included in the simulations (temperature everywhere = 300 K and the

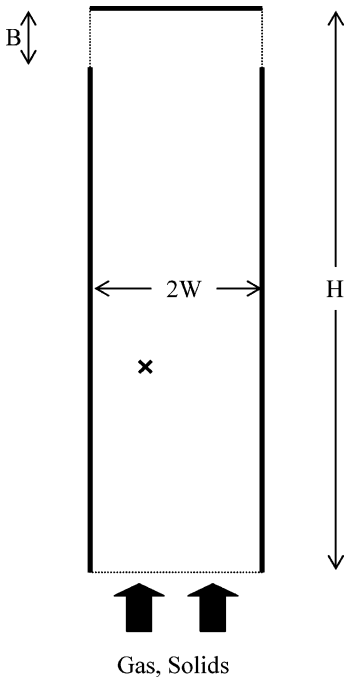

Figure 2. Schematic diagram showing the geometry used in 2D coarse grid simulations. Riser half-width, $W = 78.1$; Riser height, $H = 6164$; exit opening height, $B = 102.7$ (all in dimensionless units). Volume fraction of particles at the inlet = 0.04. Simulations were done using 38 × 375 grids. The location designated by "X" will be referred to later.

gas molecular weight = 29.0). The aspect ratio of the grids used in the coarse grid simulations was 4, and the Froude number based on the grid width, Fr_h, was 0.2434. These are exactly the same as the values of A and Fr_h used in the subgrid closure calculations outlined in the previous section.

An overview of the simulations results described below is as follows. We will first consider one simulation involving time-averaged subgrid closures and examine if separation of time scale exists between the fluctuations resolved in the coarse-grid simulations and the highly resolved simulations in small periodic domains described earlier (which are taken to be representative of the subgrid scale fluctuations). This analysis will reveal that clear separation of time scales between the resolved and unresolved fluctuations does not exist. We will therefore construct a simple stochastic subgrid closure for the drag coefficient alone (as the drag force and body force due to gravity are the two most dominant terms on the right-hand side of the vertical momentum balance for the particle phase) and examine the changes in the resolved flow structures brought about by the addition of the stochastic element. It will become clear that the differences between the resolved flow structures obtained with the time-averaged and stochastic subgrid closures are only quantitative and not qualitative. In contrast, it will be seen that when no subgrid closures are included, vastly different resolved flow characteristics are predicted in this test problem. We will then examine the sensitivity of the simulation results to changes in the wall boundary conditions. After describing all the simulation results, we outline (in the Discussion section) a plausible explanation for the observations made in our simulations.

The coarse-grid model retains the general form presented in eqs 1−4. The fluid phase stress tensor is still given by (6). The interphase interaction force is written as $f = \bar{\beta}(u - v)$, where $\bar{\beta}$ is given in Table 3. The effective particle phase pressure is now written as $\sigma_s = P_{s,meso}\underline{\underline{I}} - 2\mu_{s,meso}\underline{\underline{S}}$, and the expressions for $P_{s,meso}$ and $\mu_{s,meso}$ are summarized in Table 3. Strictly speaking, the subgrid scale horizontal and vertical normal stresses are not equal. But, as the contribution of the effective particle phase normal stress to the vertical momentum balance is negligibly small compared to the gravity and drag force terms, one can, to a good approximation, ignore the particle phase normal stress in the vertical direction in the simulations. We have ignored only the anisotropy and simply used the subgrid closure for the horizontal normal stress as $P_{s,meso}$ in both directions.

Agrawal et al.[20] have already shown through quantitative examples that, for the type of two-phase flow problems addressed here, the contribution from the gas-phase deviatoric stress—both laminar and turbulent contributions—is negligible when compared to that due to the particle phase. Therefore, we did not include any subgrid correction for the effective viscosity of the gas phase.

Very little is known about appropriate wall boundary conditions in *coarse-grid* simulations of densely loaded gas-particle flows. In high-velocity flows of densely loaded gas-particle mixtures through vertical pipes, the shear stress transmitted through the particle phase is generally much larger than that due to the gas; indeed, numerical experiments suggest that there is hardly any difference between results obtained with no-slip and free-slip boundary conditions for the gas phase. Thus, in the class of problems addressed here, the gas-phase boundary condition at the walls is not a critical factor. Visual observations of flows through vertical pipes indicate that particles do slip near the wall, and hence a partial or free-slip boundary condition for the particle phase is indicated. It is generally believed that in high-velocity flows of densely loaded gas-particle mixtures through large risers the vertical pressure gradient is largely due to the particle holdup and that wall shear is only weakly relevant.[33] Thus, the correct boundary condition for the large channel flow problem studied here is quite possibly a partial-slip condition, which is not far from a free-slip boundary condition. In the simulations described in this manuscript, we have examined both no-slip and free-slip boundary conditions for the particle and gas-phases at the bounding walls. These two extremes serve as bounds (within which the true boundary condition should lie) and thus give an idea about the extent of the changes in the mean flow characteristics that can come about upon altering the boundary conditions. It also helps us assess whether the need for (and the influence of) subgrid corrections is dependent on the wall boundary conditions employed.

Agrawal et al.[20] noted that the kinetic theory stresses were dwarfed by the mesoscale corrections when Fr_p exceeded Fr_h by a factor of ~100, which is indeed the case here. Consequently, one need not consider the fluctuation energy equation at all in the coarse-grid simulations. Therefore, the issue of appropriate boundary conditions for the granular energy equation becomes irrelevant for the present coarse-grid simulations.

The coarse-grid simulation was always carried out for a long duration (typically several thousand units of dimensionless time) and a statistical steady state was allowed to establish itself before data on various flow characteristics were gathered. The time-averaged data

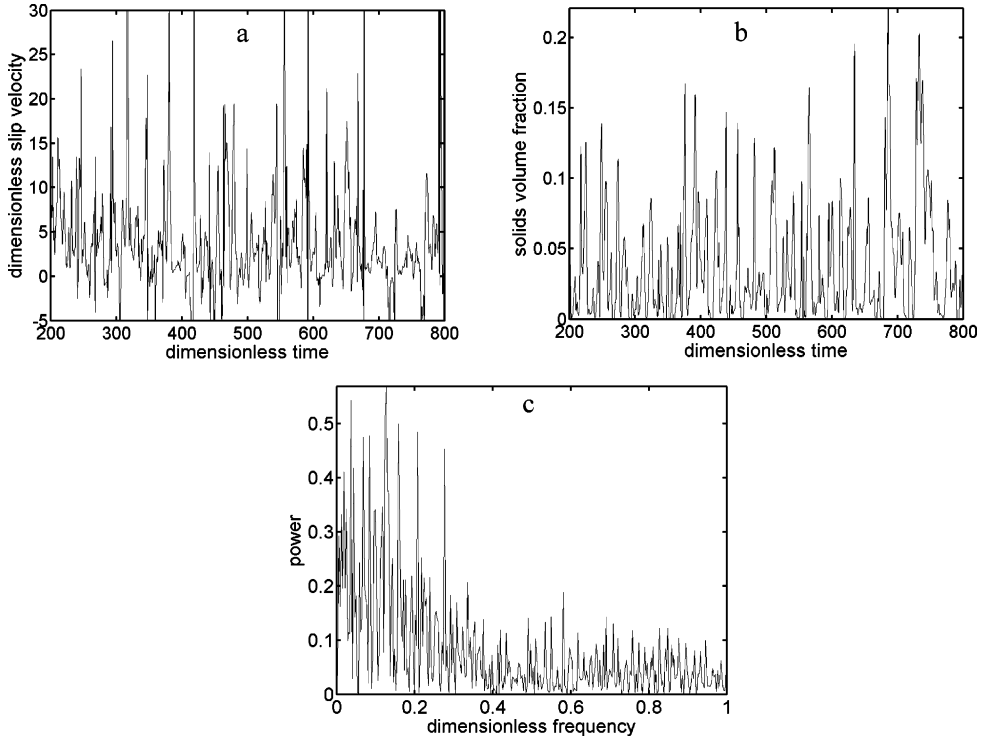

Figure 3. Results obtained from a coarse grid simulation with no-slip boundary conditions and time-averaged subgrid closures for drag coefficient and the stresses. (a) Dimensionless slip velocity and (b) particle volume fraction as functions of dimensionless time at the location marked as X in Figure 2. (c) The power spectrum of slip velocity shown in Figure 3a.

presented here were obtained by averaging the simulation results over ~3000 dimensionless units of time.

Analysis of Separation of Time Scales. Figure 3a,b shows the time dependence of the slip velocity between the gas and particle phases and the particle volume fraction at an arbitrarily chosen location in the riser. This location, marked as X in Figure 2, is 86.3 dimensionless units of length away from the left side riser wall and at an elevation of 2301 dimensionless units of length from the bottom inlet. In these simulations, we assumed no-slip conditions for both the gas and particle phases on the side walls. As expected, persistent fluctuations in all the dependent variables were observed throughout the Riser—Figure 3a,b are typical examples. Figure 3c shows the power spectrum corresponding to the results shown in Figure 3a. Although a single dominant frequency could not be identified from this figure, the range of frequencies over which most of the fluctuations occurred in the coarse-grid simulations could readily be identified. Very similar results were obtained in coarse-grid simulations using free-slip boundary conditions (discussed later). Thus, the fluctuations seen here are *not* due to the same mechanism that drives turbulent pipe flow of a single-phase fluid.

To examine if there was indeed a separation of time scale between the subgrid scale simulations (Figure 1) and the coarse-grid scale simulations (Figure 3), we present in Figure 4 further details of a representative subgrid scale simulation. The simulation conditions are exactly as in Figure 1. Figure 4a shows the instantaneous domain-averaged drag coefficient (related inversely to the slip velocity shown in Figure 1) as a function of dimensionless time. The characteristic time used to make the results dimensionless is exactly the same in subgrid and coarse-grid simulations. Figure 4b shows the power spectrum corresponding to Figure 4a. It is readily apparent from a comparison of Figures 3c and 4b that the range of dimensionless frequencies is comparable in both cases. Thus, there is no basis for ignoring in the coarse-grid simulations the fluctuations in the subgrid drag coefficient. In other words, the use of a time-averaged subgrid model for effective drag coefficient is, in a formal sense, incorrect.

This lack of separation of time scales suggests that the fluctuations observed in the subgrid and coarse-grid simulations are driven by the same mode of instability. Given that the subgrid scale simulations considered only the fluidization instability, it is reasonable to attribute the persistent fluctuations seen in the coarse-grid simulations to a local instability associated with particle phase inertia, gravity, and the dependence of the drag coefficient on particle volume fraction. In this physical picture, small-scale structures arise as a result of local instabilities and coalesce to produce large scale fluctuations observed in coarse-grid simulations.

In subgrid simulations (such as those shown in Figures 1 and 4), mesoscale structures are repeatedly formed and destroyed, and the fluctuations in the slip velocity (and other mesoscale quantities) are tied to the fluctuations in the configuration of the mesoscale structure. Thus, the need to include the effect of subgrid drag coefficient fluctuations in the coarse-grid simulations can be interpreted as a need to recognize the fact that the instantaneous subgrid mesoscale structure can vary about a mean configuration. It then follows that a proper subgrid model for the fluctuations should try to capture the evolution of the subgrid structure. As this structure is being convected by the flow, it is reasonable to anticipate that a full-fledged subgrid model for the fluctuations should be a dynamic model including convective derivatives. Such a dynamic model is rather complex and we have not pursued it in the present study. Instead, we consider a very simple localized subgrid closure that treats the fluctuations in the

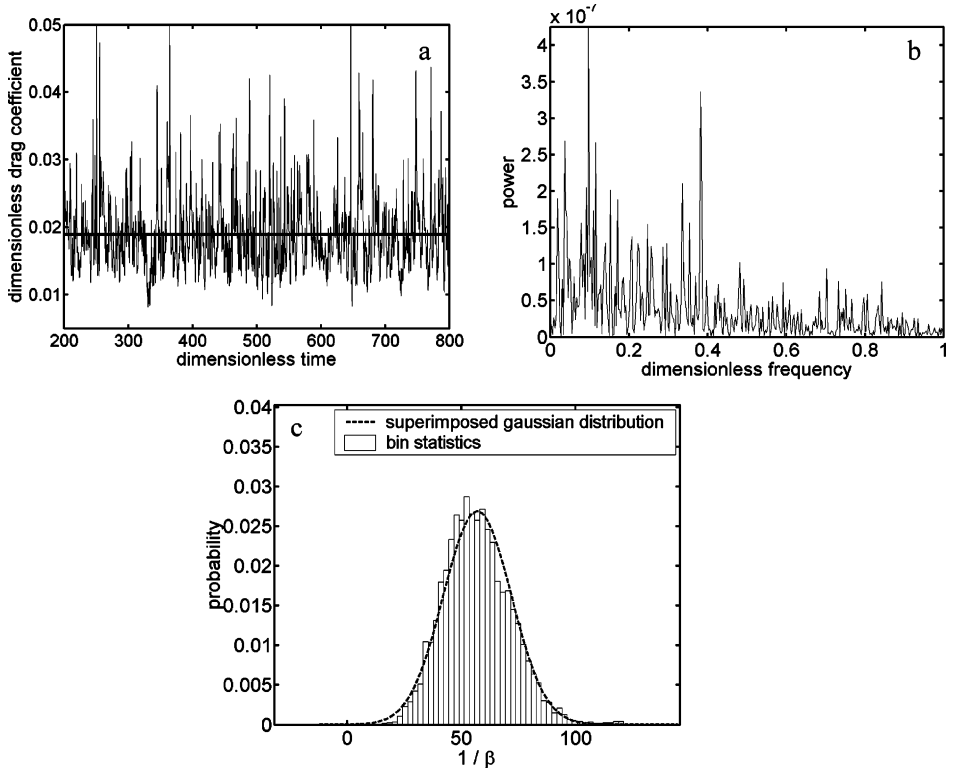

Figure 4. (a) Dimensionless drag coefficient, β_{meso}, vs dimensionless time. (b) Power spectrum of drag coefficient shown in Figure 4a. (c) Probability distribution function vs $(1/\beta_{\text{meso}})$ corresponding to Figure 4a. Geometry and conditions are the same as in Figure 1.

effective drag coefficient (see Figure 4a) as a random stochastic event.

Figure 4c shows that the probability distribution function (pdf) for $(1/\beta_{\text{meso}})$ in the statistical steady state, corresponding to the results presented in Figure 4a, is essentially Gaussian. This Gaussian distribution suggests that the formation and breakup of clusters and streamers, which drive the fluctuations in the drag coefficient, are essentially uncorrelated random events. Figure 4c suggests that, as a simple approximation, one can write

$$\left(\frac{1}{\beta_{\text{meso}}}\right) = \left(\frac{1+f}{\bar{\beta}}\right)$$

where f is a zero-mean Gaussian random variable with suitably chosen variance, and $\bar{\beta}$ is the average drag coefficient shown in Figure 4a by the horizontal line. The broken line shown in Figure 4c confirms that such a functional representation does capture the pdf.

Stochastic Subgrid Closure

To examine the possible consequence of the lack of separation of time scales between the coarse-grid and subgrid fluctuations, we constructed a simple, ad hoc time-dependent subgrid closure for the effective drag coefficient. Accordingly, the drag coefficient at each node of the coarse-grid simulation was treated as an independent stochastic random variable modeled via an Ornstein−Uhlenbeck (O−U) process.[34] The O−U model is a very simple representation of stationary stochastic fluctuations. The choice of the O−U model has precedent in single-phase turbulence where, for example, it is used to model the time evolution of a fluid particle velocity in isotropic turbulence.[35] The value of O−U model in simulating physical processes lies in its ability to produce a random stationary fluctuation with a Gaussian distribution.

In our analysis, the instantaneous drag coefficient, $\beta_{\text{meso},j}(t)$, of the jth node was written as

$$\left(\frac{1}{\beta_{\text{meso},j}}\right) = \left(\frac{1+f_j(t)}{\bar{\beta}(\phi_j(t))}\right)$$

where $\phi_j(t)$ is the instantaneous particle volume fraction at that node, $\bar{\beta}$ is the subgrid closure for the time-averaged drag coefficient, and f_j is a stochastic random variable with zero-mean. The (O−U) model to evolve a stochastic random variable f can be summarized as follows.

If f_t denotes the value of a random variable f at time t, its value at time $t + \Delta t$, $f_{t+\Delta t}$, is set to be $f_{t+\Delta t} = (\alpha_1)f_t + (\alpha_2\sigma)Rn$, where $\alpha_1 = \exp(-\Delta t/\tau^*)$ and $\alpha_2 = \sqrt{1-\alpha_1^2}$. Here τ^* and σ are model parameters; Rn is a random number with a Gaussian distribution, $\langle Rn\rangle = 0$, and $\langle Rn^2\rangle = 1$. The random variable f, evolved in time according to this rule, satisfies $\langle f\rangle = 0$, $\langle f^2\rangle = \sigma^2$ and $\langle f_t\, f_{t+\Delta t}\rangle = \sigma^2 \exp(-\Delta t/\tau^*)$, where $\langle\ \rangle$ denotes time averaging.

The stochastic model parameters τ^* and σ represent fluctuation time scale and standard deviation, respectively. The latter was taken to be the standard deviation of the mesoscale drag coefficient computed through the highly resolved simulations (see Figure 4c); an estimate of the former was obtained as the inverse of the dominant frequency of the highly resolved simulations (see Figure 4b). Figure 5 illustrates the stochastic subgrid closure for drag coefficient, applied to the conditions simulated earlier in Figure 4. The O−U model fluctuations appear (to the eye) to be similar to those seen in the detailed subgrid scale flow simulations in amplitude, frequency, and probability distribution.

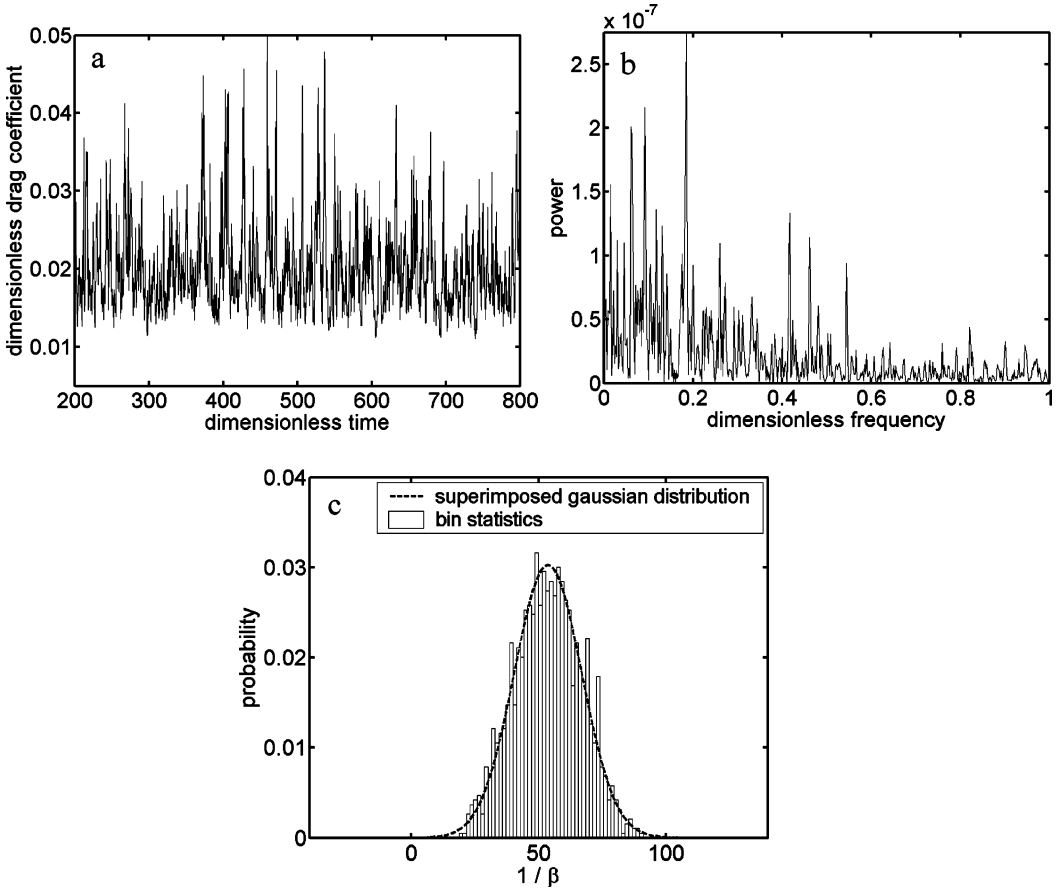

Figure 5. Temporal fluctuations in drag coefficient modeled as a Ornstein−Uhlenbeck process. O−U model parameters: characteristic time, $\tau^* = 1.12$ dimensionless time units; $\sigma = 0.25$. Particle volume fraction = 0.05. The time-averaged drag coefficient is set to be the same as that in Figure 4a. (a) Dimensionless drag coefficient, β_{meso}, vs dimensionless time. (b) Power spectrum of drag coefficient shown in Figure 5a. (c) Probability distribution function vs ($1/\beta_{meso}$) corresponding to Figure 5a.

Thus, it is reasonable to hope that such a stochastic subgrid closure for the drag coefficient can be used as a simple vehicle to investigate the possible effect of lack of separation of time scale between the subgrid and coarse-grid simulations. We found that the standard deviation σ and the characteristic time τ^* varied somewhat with particle volume fraction. However, for the sake of simplicity, we have assumed in the coarse-grid simulations described below that they are approximately constant [$\sigma = 0.25$; $\tau^* = 1.12$, both being dimensionless], as this is sufficient to investigate the consequences of lack of separation of time scales.

In what follows, when we talk about coarse-grid simulations with a *stochastic* subgrid closure for riser flows, we refer to coarse-grid simulations employing a stochastic subgrid closure for the drag coefficient along with time-averaged subgrid closures for particle-phase pressure and viscosity. Strictly speaking, we should have also included stochastic closures for the viscosity and the particle phase pressure as well. In the present study we considered a stochastic closure *only* for the drag coefficient, as the interphase interaction force term, particle inertia, and the gravitational force term are the most dominant terms in the vertical momentum balance for the particle phase. Changes to the particle phase stress term are therefore likely to have only secondary effects but could introduce computational problems; for example, instantaneous values of stochastically varying effective particle phase viscosity could be negative (although the time-averaged value is always positive), and negative viscosities may cause computational difficulties. With this in mind, we did not consider in this study stochastic fluctuations in the stresses.

Similarly, when we discuss coarse-grid simulations using a *time-averaged* subgrid closure, we refer to coarse-grid simulations employing time-averaged subgrid closures for the drag coefficient and particle-phase pressure and viscosity. Finally, coarse-grid simulations with *no* subgrid closure refer to results obtained by simply solving the microscopic equations (kinetic theory model) on a coarse grid without including any subgrid correction.

Coarse-Grid Simulations with Different Subgrid Closures

We repeated the coarse-grid simulation described earlier in Figures 2 and 3, using the stochastic subgrid closure, again using no-slip boundary conditions for both phases. We also performed an identical simulation where no subgrid corrections were made. Figure 6a−c obtained with the stochastic subgrid closure is analogous to Figure 3a−c discussed earlier in the context of time-averaged subgrid closure.

It is clear that the addition of a stochastic fluctuation in the drag coefficient has not produced any qualitative difference in the fluctuations. Instantaneous snapshots of particle volume fraction profiles between these two closures also appeared qualitatively similar (to the eye)—compare parts a and b of Figure 7. The same was true for the velocity fields as well. Thus, no qualitatively new feature appeared in the simulation results because of the addition of the stochastic correction.

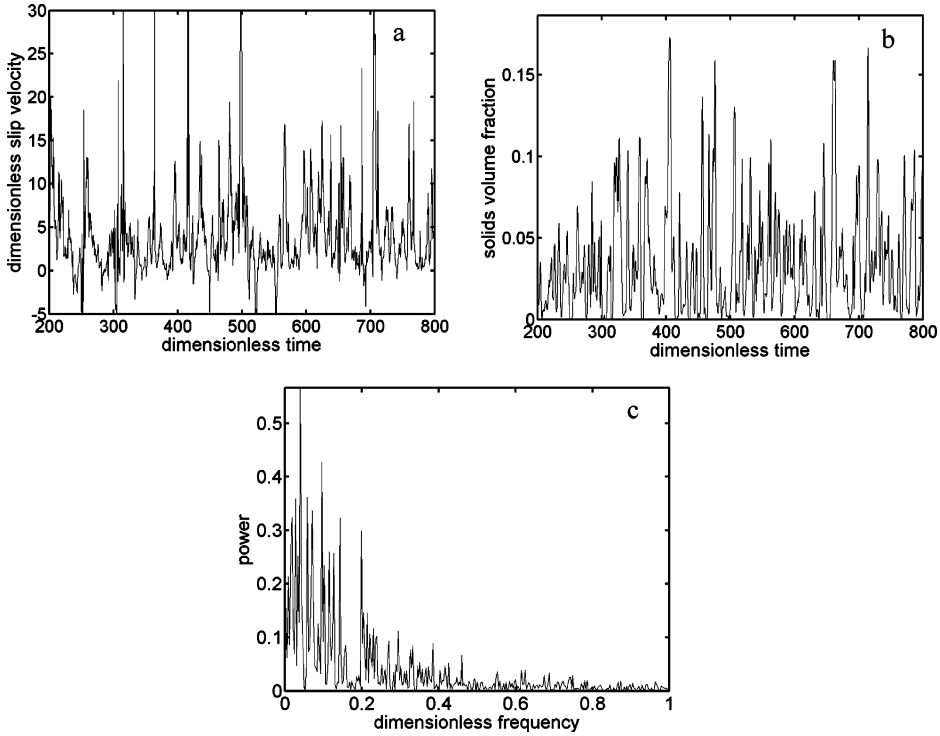

Figure 6. Results obtained from a coarse grid simulation with stochastic subgrid closure for drag coefficient and time-averaged subgrid closures for the stresses. (a) Dimensionless slip velocity and (b) particle volume fraction as functions of dimensionless time at the location marked as X in Figure 2. (c) The power spectrum of slip velocity in Figure 6a.

Surprisingly, however, when no-subgrid closure was included, large-scale nonuniformities could not be sustained even if we began our simulations with highly nonuniform initial conditions in the riser. For example, we carried out coarse-grid simulations using a stochastic subgrid closure and allowed a statistical steady state to evolve. We then stopped the simulation at different times in the statistical steady state, turned off the subgrid closure, and continued the simulation. We found that over a few multiples of the residence time in the riser the inhomogeneities washed out of the riser, and a nearly homogeneous state with small fluctuations resulted. Thus, in this example, inhomogeneities could not be sustained without adding subgrid closures.

From our coarse-grid simulations, we have obtained the time-averaged profiles of various quantities in the statistical steady state, some of which are illustrated below. Figure 8 shows the laterally averaged particle volume fraction as a function of riser elevation for the three cases: no subgrid, time-averaged subgrid, and stochastic subgrid closures. We performed simulations with two different initial conditions, one where the channel was initially devoid of particles and another where the channel was initially filled with a nonuniform distribution of particles. The time-averaged results representing a statistical steady state showed no significant dependence on the initial condition. (Some small difference was invariably present; however, as the difference decreased with increasing sampling time, it was taken as an indication that the data had not been averaged for a sufficiently long duration.)

The result obtained in the *no subgrid closure* case is qualitatively different from those in the other two cases. It proved to be deficient in the sense that it did not reproduce the generally known, large-scale fluctuations. Coarse-grid simulations without any subgrid closures may produce inhomogeneous and fluctuating flow structures, when asymmetries are present at the inlet and

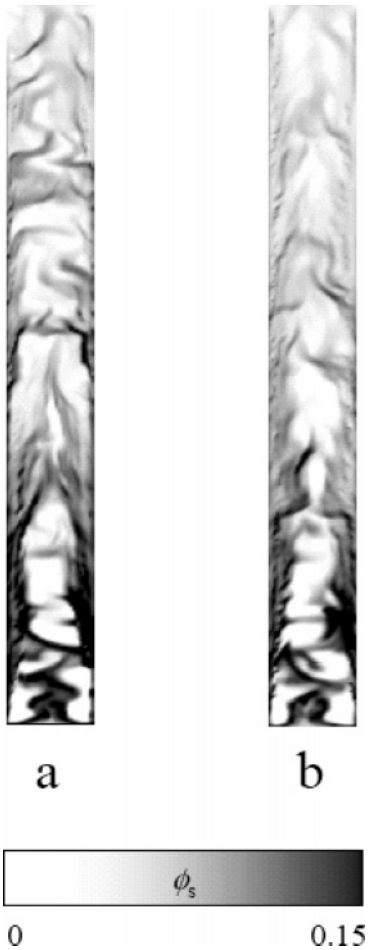

Figure 7. Snapshots of particle volume fractions obtained in the coarse-grid simulations: (a) time-averaged subgrid closure and (b) stochastic subgrid closure. No-slip boundary conditions for both phases.

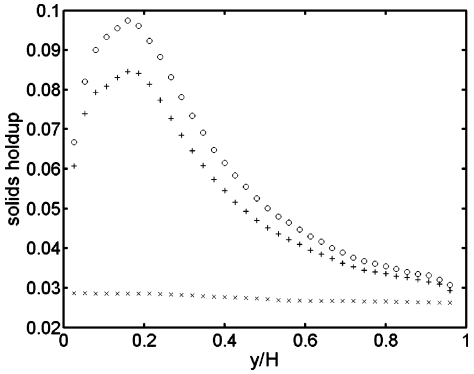

Figure 8. Axial variation of laterally averaged particle volume fraction corresponding to statistical steady state. Results obtained from coarse-grid simulations with stochastic (+) and time-averaged (o) subgrid closures are compared. Also shown as (x) are results corresponding to kinetic theory (i.e. with no subgrid closures). No slip boundary conditions. Uniform inlet conditions. The riser geometry and conditions are the same as in Figures 2 and 3.

outlet. The influence of the inlet and exit configurations on the riser flow characteristics is a question of significant practical concern, but investigation of this influence is not the goal of the present study. We do not believe that such asymmetries are essential to produce sustained fluctuations inside the riser. It is also important to spell out what is meant when we say that the results are deficient. This does not mean that the microscopic models are deficient. Our expectation is that highly resolved simulations of the set of equations described in Table 1 would afford sustained fluctuations; the deficiency is purely associated with inadequate grid resolution.

The axial profiles for the other two cases (i.e. with time-averaged and stochastic subgrid closures) manifest peaks in the laterally averaged particle volume fraction at an intermediate elevation in the riser (~15% of riser height from the bottom). In simulations with both the time-averaged and stochastic subgrid closures, particle rich regions are more commonly seen near the wall, and they slowly descend, causing an accumulation near the bottom of the riser. However, the upward flow from the inlet tends to push the accumulated solids upward, and these two opposing effects are responsible for the peak at the intermediate elevation. It is clear from Figure 8 that the time-averaged and stochastic subgrid closures lead to quantitatively different results near the inlet but converge at higher riser elevations. Figure 9 shows the lateral profiles of particle volume fraction and dimensionless particle flux at an elevation of 80% of the riser height, where the laterally averaged particle volume fractions obtained with the stochastic and time-averaged subgrid closures are fairly close. Both closures predict enrichment of particle concentration and downflow near the wall region. The results are quantitatively different, but the difference is not very large. Although we do not attempt any comparison with experimental data in this study, we suspect that the uncertainties in the experimental data will be at least as large as the differences between these two closure predictions and that discrimination between these two closures by comparison with experimental data in the upper elevation of risers is unlikely. On the other hand, discrimination may be possible at the lower elevations. However, the details of flow at the bottom are probably very sensitive to the spatial nonuniformities and fluctuations in the inlet flow (discussed later), and proper discrimination between

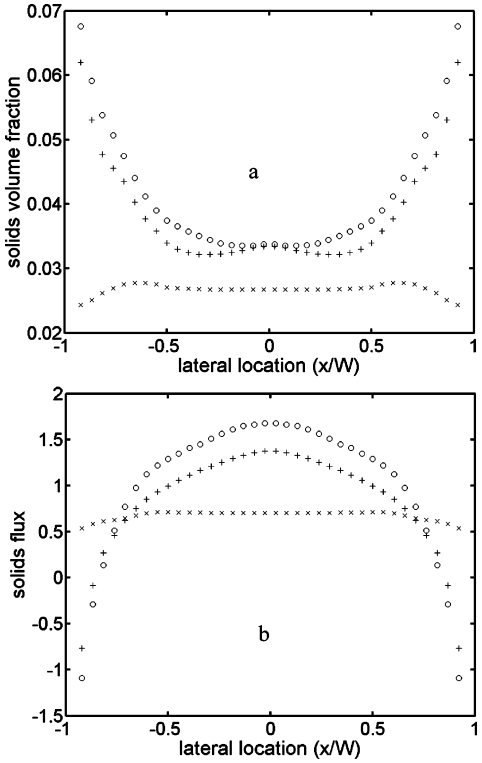

Figure 9. Lateral variations of (a) particle volume fraction and (b) dimensionless particle flux at an elevation of 80% of the riser height. Results obtained from coarse-grid simulations with stochastic (+) and time-averaged (o) subgrid closures are compared. Also shown as (x) are results corresponding to kinetic theory (i.e. with no subgrid closures). No slip boundary conditions. Uniform inlet conditions. The riser geometry and conditions are the same as in Figures 2 and 3.

closures on the basis of experimental data will be difficult unless one carefully measures the inlet flow characteristics.

In any case, there is no doubt that the addition of a subgrid closure (be it the time-averaged subgrid closure or the stochastic subgrid closure) has dramatically altered the simulation results in this test problem.

Coarse-Grid Simulations with Free-Slip Boundary Conditions

As discussed earlier, no-slip boundary condition at the solid walls (used in the simulations described above) is by no means accurate, and a partial slip boundary condition (which is not too far from free slip) is probably more realistic. We explored the sensitivity of the coarse grid simulation results to the wall boundary conditions by repeating a number of simulations using free slip boundary conditions for both phases. Specifically, we started from a highly nonuniform initial state obtained via coarse grid simulation using the time-averaged or the stochastic subgrid closure and no-slip boundary conditions and continued the simulation with free slip boundary conditions and desired subgrid closure. Once again, the fluctuations were washed out of the channel when no subgrid closure was included. With the time-averaged and stochastic subgrid closures, fluctuations persisted. Figure 10a,b shows snapshots of simulations with free slip boundary conditions; no dramatic, qualitative difference between the time-averaged and stochastic subgrid closures is apparent. Indeed, these snapshots are not much different from those obtained

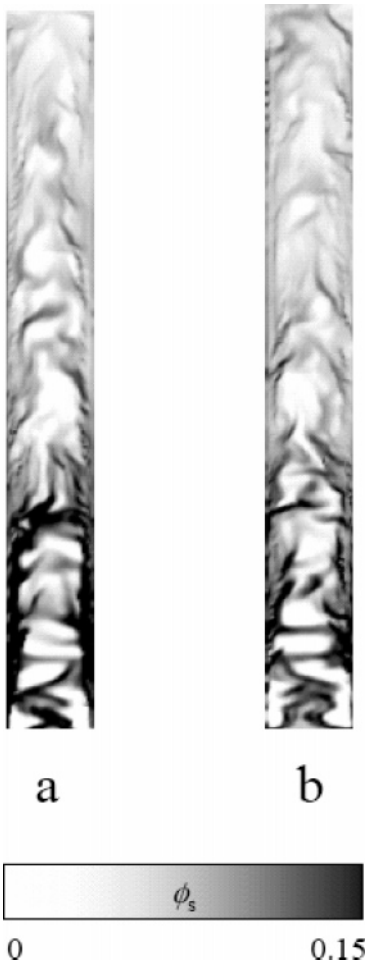

Figure 10. Snapshots of particle volume fractions obtained in the coarse-grid simulations: (a) time-averaged subgrid closure and (b) stochastic subgrid closure. Free-slip boundary conditions for both phases.

with no-slip boundary conditions, suggesting that the gross features of the fluctuating flow pattern in a statistical steady state are not driven by specific choice of wall boundary conditions.

Coarse grid simulations with free slip boundary conditions manifested sensitivity to the initial condition. When the above simulations were repeated, starting from an initially empty channel, nonuniform distribution of particles and persistent large-scale fluctuations in particle concentration did not develop with both subgrid closures. This suggested that there are at least two attractors for simulations with free slip boundary conditions. Such a multiplicity has not been reported in any experimental study and is therefore likely to be unphysical. In practice, the inlet at the bottom is neither perfectly uniform nor steady, and spatial nonuniformities and temporal fluctuations are inevitable at the bottom inlet. Indeed, when we introduced stochastic, lateral variation in axial particle mass flux at the inlet to a simulation with stochastic subgrid closure, the nonuniform distribution of particles and persistent large-scale fluctuations readily developed even from a uniform initial condition.[36] Thus, nonuniformities or fluctuations at the inlet and/or some resistance at the solid walls to flow serve to eliminate spurious solutions.

Figure 11 presents the axial variation of laterally averaged particle volume fraction in the statistical steady state for simulations with free slip boundary conditions, a highly nonuniform initial condition, and

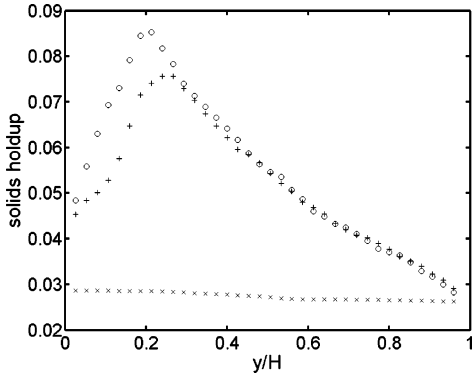

Figure 11. Axial variation of laterally averaged particle volume fraction corresponding to statistical steady state. Results obtained from coarse-grid simulations with stochastic (+) and time-averaged (o) subgrid closures are compared. Also shown as (x) are results corresponding to kinetic theory (i.e. with no subgrid closures). Free-slip boundary conditions. Uniform inlet conditions. The riser geometry and conditions are the same as in Figures 2 and 3.

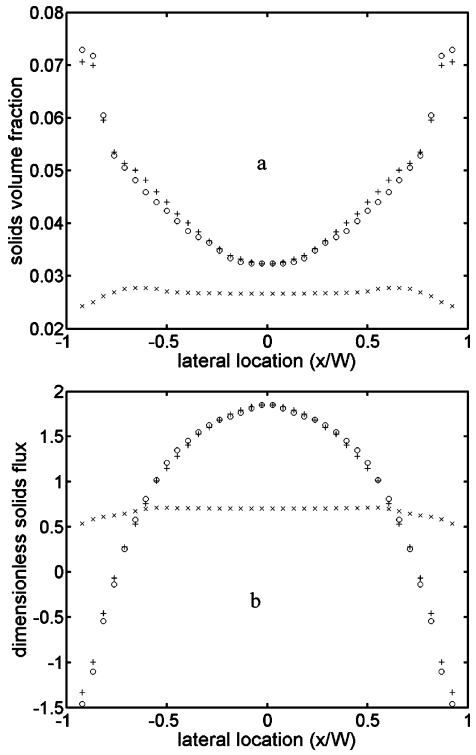

Figure 12. Lateral variations of (a) particle volume fraction and (b) dimensionless particle flux at an elevation of 80% of the riser height. Results obtained from coarse-grid simulations with stochastic (+) and time-averaged (o) subgrid closures are compared. Also shown as (x) are results corresponding to kinetic theory (i.e. with no subgrid closures). No slip boundary conditions. Uniform inlet conditions. The riser geometry and conditions are the same as in Figures 2 and 3.

uniform inlet. Once again, we see that the results obtained with the time-averaged and stochastic subgrid closures are qualitatively similar, while the result obtained in simulations with no subgrid correction is grossly different. Comparison of Figures 8 (no slip) and 11 (free slip) reveal no qualitative differences; however, the wall boundary conditions do seem to have a quantitative effect on the predicted holdup profile.

Figure 12a,b shows lateral variation of particle volume fraction and dimensionless particle flux at an elevation of 80% of riser height. It is clear that the time-averaged and stochastic subgrid closures yield nearly

the same results. Comparison of these figures with Figure 9a,b reveals that a change in wall boundary conditions *does* lead to quantitative changes.

Discussion

Our simulations show clearly that the dominant fluctuations occurred at comparable dimensionless frequencies (which are much smaller than the inverse of dimensionless time step) in both coarse-grid and mesoscale calculations. This suggests that fluctuations derive from the same process at both scales. As fluctuations do occur in mesoscale simulations even in the absence of macroscale shear and in coarse-grid simulations with free-slip boundary conditions, let us begin by examining instabilities associated with the governing equations of motion without requiring an active role for the macroscale shear or exit configuration. In the absence of shear and exit effect, the governing equations support a simple solution where the gas-particle mixture travels up the channel homogeneously with the slip velocity being adequate to support the weight of the particle—that is, the simplest version of riser flow is a vertically traveling homogeneous fluidized bed. It is well-known that the dominant instability in homogeneously fluidized beds, as predicted by the averaged equations of motion with simple phenomenological closures where the particle phase pressure and viscosity are only functions of particle volume fraction, take the form of one-dimensional, vertically traveling wave fronts having no horizontal structure.[37] Two-dimensional linear stability analysis of a uniformly fluidized bed of infinite extent based on the microscopic (kinetic theory) equations used in the present study[28] revealed that the most unstable mode is an oblique wave, with the horizontal wavenumber being much smaller than the vertical wavenumber. Hence it is sufficient to focus our discussion on growth rates of vertically traveling wave fronts having no horizontal structure and the amplification of disturbances introduced at the bottom of the riser and convected upward by the flow. The time available for amplification is comparable to the residence time of the mixture in the riser.

According to the microscopic (kinetic theory) equations, the homogeneously fluidized state is unstable to vertically traveling horizontal wave fronts whose wavelength is larger than a few particle diameters, and the dominant mode has a wavelength of 10 or so particle diameters[28] (also see Appendix A). The growth rate of perturbations whose wavelength is much larger than that of the dominant mode is *much* smaller than that of the dominant mode. Thus, a homogeneously fluidized bed gives way to nonuniform structures in coarse-grid simulations much more slowly than in highly resolved simulations (also see Appendix C for further comments on differences between growth rates of various modes in the continuum equations and in the discretized equations). As a result, appreciable amplification of the initial disturbances (which, in turn, can give way to lateral nonuniformities through secondary gravitational overturning instability[18,38−40]) does not occur in the coarse-grid simulations with free-slip boundaries within the time available in the riser flow and the disturbance gets washed out of the riser. Our observation that a highly nonuniform initial state (coupled with uniform inlet conditions) could not sustain the fluctuating state suggests that the basin of attraction for the homogeneous state is fairly large and/or that a fluctuating statistical steady state does not exist for the microscopic equations discretized on a coarse grid.

When modest stochastic, lateral variation was introduced in axial particle mass flux at the inlet, the fluctuations persisted in the riser (in our simulations of the microscopic equations discretized on a coarse grid coupled with free-slip boundary conditions); however, the time-averaged solution was only marginally different from that obtained without stochastic fluctuations, clearly suggesting that this solution was only a mild perturbation of the homogeneous solution.

Note that in our riser simulations the gas-particle mixture entered the riser in a plug flow manner. When no-slip boundary conditions are employed, both the fluid and the particles are forced to slow near the wall and an increase in particle volume fraction must occur purely because of kinematic effect. This represents another form of lateral nonuniformity that can, in principle, develop into a fluctuating state. However, the particle phase viscosity in the homogeneous state is very small (when no subgrid correction is included). Therefore, the boundary layer near the channel walls did not grow rapidly with distance from the inlet in our coarse-grid simulation examples (without any subgrid correction) and the particle concentration near the channel walls did not grow appreciably with height. Thus, lateral perturbation to the homogeneously fluidized state by the presence of the sidewalls was not large enough to give rise to and sustain the highly nonuniform fluctuating state.

Our computational experiments indicate that nonuniform solutions with sustained fluctuations and lateral segregations *may* develop in coarse-grid simulations of the microscopic equations only if pronounced asymmetry or nonuniformity is present at the inlet (such as side entrance, large scale fluctuations at the inlet, etc.).

The addition of the time-averaged closure expressions in Table 3 to the microscopic closure equations affects the growth rate of linear modes in at least two ways. As increase in the particle phase viscosity (brought about by the addition of the subgrid scale viscosity) decreases the growth rate, while the subgrid correction to the drag coefficient tends to increase the growth rate. Our observation that the fluctuating state could not be reached from uniform initial conditions (and uniform inlet conditions) when time-averaged subgrid closures were used along with free slip boundary conditions suggests that the difference in the outcome of the coarse-grid simulations with and without subgrid closures is *not* due to a larger growth rate of disturbances in the presence of subgrid closures. The observation that the fluctuating state could be sustained (even with free-slip boundary conditions) if the simulations began with a nonuniform initial condition reveals coexistence of a homogeneous solution and a high-amplitude nonuniform solution. [Such coexistence of solutions for these equations has been demonstrated previously, see refs 39 and 40.] We found that adding stochastic, lateral fluctuations in particle mass flux at the inlet to simulations with time-averaged subgrid closures and free slip boundary conditions could eliminate the homogeneous state; thus, the homogeneous solution appears to have only a small attractor basin. When no-slip boundary conditions are used in the simulations using subgrid corrections, the boundary layer grows more rapidly than in the no subgrid case, as the particle phase viscosity is much larger when a subgrid closure is used. Conse-

quently, particle accumulation near the wall region is more pronounced when a subgrid closure is used, and this lateral nonuniformity is apparently enough to take the system into the basin of attraction for the fluctuating state.

It should be noted that, in the present study, we do not address spatial scales. Agrawal et al.[20] examined the microstructure over regions of different sizes and found that the size of the clusters increased with larger regions. In our present coarse-grid simulations, we do resolve structures that span over several grid lengths. Thus, almost definitely, there is no clear separation of spatial scales in these flow problems. In fact, this is a typical character of many multiphase flows, where there is no clear temporal or spatial scale separation. There is, however, some evidence of similarity in the spatial scale, as demonstrated by Agrawal et al.,[20] who found that plots of effective slip velocity (which is inversely related to the effective drag coefficient) vs particle volume fraction for different region sizes manifested similar shapes.

There are a number of other issues which must be explored in future studies, such as the effect of the size of the coarse grids on the simulation results, and the differences between 2-D and 3-D simulations, before the simulation results can be compared with experimental data. Until these issues are addressed, good agreement between simulations and experimental data does not mean anything. A fruitful approach to validating the coarse-grid simulation approach would be to generate *computational data* of flow in a fairly large domain through highly resolved simulations of the microscopic equations and compare the predictions of the coarse-grid simulations of the same set of microscopic equations augmented with its corresponding subgrid closures against these computational data. Such highly resolved simulations are expensive and beyond the scope of the present study but are essential for validation of the approach described in this study. These highly resolved simulations will also aid in developing fundamentally based subgrid models.

Summary

It is clear from the examples presented here that the results obtained in coarse-grid integration of the microscopic equations for gas-particle flows in large process vessels can change appreciably if subgrid corrections to account for the effects of unresolved structures are included. The most dramatic difference occurred in our simulations when a simple *time-averaged* subgrid closure was added to the *no subgrid* closure case. Although the level of sophistication of the subgrid closure did make a difference in the quantitative results in our simulations, even a simple time-averaged subgrid closure appeared to capture the main qualitative effects.

The simple time-averaged subgrid closure is, in a strict sense, flawed, as there is no separation of time scales between the unresolved (subgrid) structures and those resolved in the coarse-grid simulations. To account for this lack of separation of time scale, a rather simple enhancement of the time-averaged subgrid closure that took the form of a stochastic correction to the drag coefficient was implemented. It was found that such a stochastic subgrid closure yielded qualitatively the same results as the time-averaged subgrid closure. Thus the lack of separation of time scales does not appear to be a severe deficiency.

The approach employed in the present study to construct subgrid closures is clearly ad hoc. Such an approach is adequate, in our opinion, for our study as our primary goal is to expose the potential importance of subgrid corrections. More in-depth study of the processes occurring at small scales is needed to develop meaningful and broadly useful subgrid closures.

It should also be emphasized that the present analysis only considered a static interphase interaction force—even though the stochastic part introduced a time-dependent character, it does not capture dynamic effects of the type examined by Zhang and VanderHeyden,[41] who argued that the mesoscale structures can lead to an appreciable added mass correction. Additional work is required to verify the existence of such a dynamic term—if it does exist, it may slow the coarse-grid fluctuations appreciably and eliminate the need for a stochastic subgrid closure for the drag coefficient.

Acknowledgment

This work was supported by the U.S. Department of Energy CDE-FC26-00NT40971. Andrews and Loezos benefited immensely from summer training at the National Energy Technology Laboratory, Morgantown, WVa, where they not only learned how to use MFIX but also incorporated into MFIX some of the new features needed for the present study. We gratefully acknowledge the assistance and insight provided to us by Madhav Syamlal (NETL), Thomas O'Brien (NETL), Chris Guenther (NETL), Sofiane Benyahia (NETL), and Sreekanth Pannala (OakRidge National Lab) throughout the course of this study.

Appendix A

The linear stability of the homogeneously fluidized state against perturbations that take the form of one-dimensional traveling wave fronts with no horizontal structure has been studied extensively in the literature (see ref 37 for a summary). This analysis reveals that, for gas fluidized beds, the wavelength corresponding to marginal stability conditions, L, scales as[38−40]

$$\frac{L}{d} \sim \left(\frac{\mu_s v_t}{\rho_s g}\right)^{1/2}$$

where μ_s is the particle phase viscosity in the homogeneously fluidized state, d is the particle size, and v_t is the terminal settling velocity of the particle. Typically,

$$\mu_s \sim \rho_s v_t d, \text{ so that } \frac{L}{d} \sim \left(\frac{{v_t}^2}{gd}\right)^{1/2}$$

For most gas-particle systems encountered in high velocity flows, such as that considered in the present manuscript, $v_t^2/gd \sim 40-100$. This leads to the ten-particle diameter estimate mentioned in the text.

Appendix B

Equations 1−4 describe the continuity and momentum balance equations for the particle and gas phases. Here, ϕ is the volume fraction of particles; v and u are the local average velocities of the particle and gas phases, respectively; ρ_s and ρ_g are the densities; σ_s and σ_g and are the stress tensors associated with the two phases expressed in a compressive sense; f is the

interaction force between the phases per unit volume of the bed; and g is the specific gravity force. Equation 5 is the pseudothermal energy (PTE) balance, where T is the granular temperature—in this equation, q is the diffusive flux of PTE; the second and third terms on the right-hand side quantify the rates of production of PTE by shear and gas-particle slip, respectively. The fourth and the fifth terms account for the rates of dissipation of PTE through inelastic collisions and viscous damping, respectively.

Equation 6 describes a simple Newtonian closure for the effective gas-phase stress. Here p_g and $\hat{\mu}_g$ denote fluid phase pressure and effective viscosity, respectively. In the regime investigated in the present study, namely, $\rho_s\phi \gg \rho_g(1 - \phi)$, the contribution due to the deviatoric part of the gas-phase stress is negligible.

The gas-particle interaction force, f, is, for all practical purposes, only due to drag. Equation 7 describes the drag correlation used in our simulations.[23] Here β, C_D, d, μ_g, and Re_g denote an effective drag coefficient for the suspension, single particle drag coefficient, particle diameter, fluid viscosity, and Reynolds number, respectively.

Equation 8 summarizes a kinetic theory closure for the particle phase stress in the fluid-particle mixture. An expanded discussion of this closure can be found in ref 20. Here e_p denotes the coefficient of restitution for particle−particle collisions, and the spheres are assumed to be smooth. Equation 9 is the corresponding closure for the diffusive flux of PTE.

Equation 10 is the kinetic theory closure for the rate of dissipation of PTE through inelastic collisions, while eq 11 represents the closure due to Koch and Sangani[19] for the rate of dissipation of PTE by viscous dissipation in the fluid phase.

Appendix C

There is a difference between growth rates of Fourier modes found through a linear stability analysis of continuum models that take the form of partial differential equations and those one would obtain from a system of ordinary differential equations generated through (spatial) discretization of the partial differential equations. This difference stems from truncation errors associated with spatial discretization. When the discretization is performed on *coarse* spatial grids, Fourier modes which are unstable in the partial differential equations can be incorrectly identified as stable modes of the ordinary differential equations.

Literature Cited

(1) Benyahia, S.; Arastoopour, H.; Knowlton, T. M. Simulation of particles and gas flow behavior in the riser section of a circulating fluidized bed using the kinetic theory approach for the particulate phase. *Powder Technol.* **2000**, *112*, 24−33.

(2) Benyahia, S.; Arastoopour, H.; Knowlton, T. M. Two-dimensional transient numerical simulation of solids and gas flow in the riser section of a circulating fluidized bed. *Chem. Eng. Commun.* **2002**, *189*, 510−527.

(3) Ding, J.; Gidaspow, D. A Bubbling Fluidization Model Using Kinetic-Theory of Granular Flow. *AIChE J.* **1990**, *36*, 523−538.

(4) Enwald, H.; Peirano, E.; Almstedt, A. E. Eulerian two-phase theory applied to fluidization. *Int. J. Multiphase Flow.* **1997**, *22*, Suppl., 21−66.

(5) Enwald, H.; Peirano, E.; Almstedt, A. E.; Leckner, B. Simulation of the fluid dynamics of a bubbling fluidized bed. Experimental validation of the two-fluid model and evaluation of a parallel multiblock solver. *Chem. Eng. Sci.* **1999**, *54*, 311−328.

(6) Enwald, H.; Almstedt, A. E. Fluid dynamics of a pressurized fluidized bed: comparison between numerical solutions from two-fluid models and experimental results. *Chem. Eng. Sci.* **1999**, *54*, 329−342.

(7) Nieuwland, J. J.; Huizenga, J. J. P.; Kuipers, J. A. M.; van Swaaij, W. P. M. Hydrodynamic modelling of circulating fluidized beds. *Chem. Eng. Sci.* **1995**, *49*, 5803−5811.

(8) Nieuwland, J. J.; Annaland M. V.; Kuipers, J. A. M.; van Swaaij, W. P. M. Hydrodynamic modelling of gas/particle flows in riser reactors. *AIChE J.* **1996**, *42*, 1569−1582.

(9) Gidaspow, D. *Multiphase Flow and Fluidization*; Academic Press: CA, 1994.

(10) Lu, H. L.; Gidaspow, D. Hydrodynamic simulations of gas−solid flow in a riser. *Ind. Eng. Chem. Res.* **2003**, *42*, 2390−2398.

(11) Goldschmidt, M. J. V.; Kuipers, J. A. M.; van Swaaij, W. P. M. Hydrodynamic modeling of dense gas-fluidized beds using the kinetic theory of granular flow: Effect of restitution coefficient on bed dynamics. *Chem. Eng. Sci.* **2001**, *56*, 571−578.

(12) Neri, A.; Gidaspow, D. Riser hydrodynamics: Simulation using kinetic theory. *AIChE J.* **2000**, *46*, 52−67.

(13) Samuelsberg, A.; Hjertager, B. Computational modelling of gas/particle flow in a riser. *AIChE J.* **1996**, *42*, 1536−1546.

(14) Sun, B.; Gidaspow, D. Computation of circulating fluidized bed riser flow for the Fluidization VIII benchmark test. *Ind. Eng. Chem. Res.* **1999**, *38*, 787−792.

(15) Tsuo, Y. P.; Gidaspow, D. Computation of flow patterns in circulating fluidized beds. *AIChE J.* **1990**, *36*, 885−896.

(16) van Wachem, B. G. M.; Schouten, J. C.; van den Bleek, C. M.; Krishna, R.; Sinclair, J. L. Comparative analysis of CFD models of dense gas−solid systems. *AIChE J.* **2001**, *47*, 1035−1051.

(17) Zhang, D. Z.; VanderHeyden, W. B. High-resolution three-dimensional numerical simulation of a circulating fluidized bed. *Powder Technol.* **2001**, *116*, 133−141.

(18) Glasser, B. J.; Sundaresan, S.; Kevrekidis, I. G. From bubbles to clusters in fluidized beds. *Phys. Rev. Lett.* **1998**, *81*, 1849−1852.

(19) Koch, D. L.; Sangani, A. S. Particle pressure and marginal stability limits for a homogeneous monodisperse gas fluidized bed: kinetic theory and numerical simulations. *J. Fluid Mech.* **1999**, *400*, 229−263.

(20) Agrawal, K.; Loezos, P. N.; Syamlal, M.; Sundaresan, S. The Role of Meso-scale Structures in Rapid Gas−solid Flows. *J. Fluid Mech.* **2001**, *445*, 151−185.

(21) Sundaresan, S. Perspective: Modeling the Hydrodynamics of Multiphase Flow Reactors: Current Status and Challenges. *AIChE J.* **2000**, *46*, 1102−1105.

(22) Lun, C. K. K.; Savage, S. B.; Jeffrey, D. J.; Chepurniy, N. Kinetic theories of granular flows: inelastic particles in Couette flow and slightly inelastic particles in a general flow field. *J. Fluid Mech.* **1984**, *140*, 223 − 256.

(23) Wen, C. Y.; Yu, Y. H. Mechanics of Fluidization. *Chem. Eng. Prog. Symp. Ser.* **1966**, *62*, 100−111.

(24) McKeen, T.; Pugsley, T. Simulation and Experimental Validation of a Freely Bubbling Bed of FCC Catalyst. *Powder Technol.* **2003**, *129*(1−3), 139−152.

(25) Yang. N.; Wang, W.; Ge, W.; Li, J. CFD Simulation of Concurrent-up Gas−Solid Flow in Circulating fluidized beds with Structure-dependent Drag Coefficient. *Chem. Eng. J.* **2003**, *96*, 71−80.

(26) O'Brien, T. J.; Syamlal, M. Particle Cluster Effects in the Numerical Simulation of a Circulating Fluidized Bed. In *Circulating Fluidized Bed Technology IV*; Avidan, A., Ed.; Proceedings of the Fourth International Conference on Circulating Fluidized Beds, Hidden Valley Conference Center and Mountain Resort, Somerset, PA, August 1−5, 1993.

(27) Boemer, A.; Qi, H.; Hannes, J.; Renz, U. Modelling of solids circulation in a fluidised bed with Eulerian approach. 29th IEA-FBC Meeting in Paris, France, Nov. 24−26, 1994.

(28) Tan, J. *2-D stability analysis of gas-particle flows in risers*, BSE Thesis, Department of Chemical Engineering: Princeton University, Princeton, New Jersey, 2000.

(29) Syamlal, M. *MFIX Documentation: Numerical Techniques*; DOE/MC-31346-5824. NTIS/DE98002029. December 1998.

(30) Syamlal, M.; Rogers, W.; O'Brien, T. J. *MFIX Documentation*; U.S. Department of Energy, Federal Energy Technology Center: Morgantown, WV, 1993.

(31) Guenther, C.; Syamlal, M. The Effect of Numerical Diffusion on Isolated Bubbles in a Gas−Solid Fluidized Bed. *Powder Technol*. **2001**, *116*, 142−154.

(32) Piomelli, U.; Balaras, E. Wall-Layer Models for Large-Eddy Simulations. *Annu. Rev. Fluid Mech*. **2002**, *34*, 349−374.

(33) Chang, H.; Louge, M. Fluid Dynamic Similarity of Circulating Fluidized-Beds. *Powder Technol.* **1992**, *70*, 259−270.

(34) Uhlenbeck, G. E.; Ornstein, L. S. On the theory of Brownian motion. *Phys Rev*. **1930**, *36*, 823−841.

(35) Pope, S. *Turbulent Flows*; Cambridge University Press: 2000; pp 720−722.

(36) Andrews, A. T. Effect of Velocity Fluctuations at the Inlet on Riser Flow Characteristics. Presented at the 2002 Multiphase Fluid Dynamics Research Consortium, Columbia, MD, 2002.

(37) Jackson, R. *The dynamics of fluidized particles*; Cambridge University Press: 2000.

(38) Batchelor, G. K. Secondary Instability of a Gas-Fluidized Bed. *J. Fluid Mech.* **1993**, *445*, 151−185

(39) Glasser, B. J.; Kevrekidis, I. G.; Sundaresan, S. One- and two-dimensional travelling wave solutions in gas-fluidized beds. *J. Fluid Mech*. **1996**, *306*, 183−221.

(40) Glasser, B. J.; Kevrekidis, I. G.; Sundaresan, S. Fully developed travelling wave solutions and bubble formation in fluidized beds. *J. Fluid Mech*. **1997**, *334*, 157−188.

(41) Zhang, D. Z.; VanderHeyden, W. B. The effects of mesoscale structures on the macroscopic momentum equations for two-phase flows. *Int. J. Multiphase Flow*. **2002**, *28*, 805−822.

Received for review August 25, 2004
Revised manuscript received February 28, 2005
Accepted March 10, 2005

IE0492193